

Source model for Immunostimulating Interstitial Laser Thermotherapy dosimetry

Emily Emilsson

Thesis submitted for the degree of Master of Science, 30 credits

Project duration: 5 months

Supervised by: Dr. Johan Axelsson & Cristina Pantaleone

Department of Atomic Physics, Lund University

Autumn 2016

March 9, 2017



LUND UNIVERSITY

Abstract

A common tool for tissue ablation is the use of heat. For the imILT^{CLS} technique investigated in this project, the heat is induced by the usage of laser light. The light is absorbed by the tissue and is thus turned into heat, the amount absorbed depends on the optical properties of the tissue, such as absorption and scattering. In imILT^{CLS} such as in other laser based ablation techniques, optical fibers are used to deliver the laser light to the treatment volume. The main aim of this project was to develop a source model for the imILT^{CLS} technique using COMSOL Multiphysics. This was done in three steps, first ray tracing inside the different fiber models, then light distribution in tissue and last heat distribution in tissue due to the introduced laser light. A second aim of this project was to simulate the heat induced in the different fiber layers during an imILT^{CLS} treatment for the different fiber designs as well as comparing two fibers of the same design but of different thicknesses. The two fiber designs used were bare end and radial. The results from the developed simulation model are in large, in agreement with the validation experiments performed. The intensity profiles of the bare end fiber is approximately the same for both simulation and experiment, but differs slightly for the radial fibers. The results from the heat distribution simulation models does agree with the validation experiments but overall, the temperatures received in the simulation may be lower than for the validations. This is most likely due to the main source of error in the simulations, the optical properties of the simulated tissue. When comparing the two fibers of the same model but different thicknesses, it was concluded that different parameters limit the maximum power and treatment time that can be used for the different fiber thicknesses.

Abbreviations

CLS	Clinical Laserthermia Systems
imILT	Immunostimulating Interstitial Laser Thermotherapy
NA	Numerical Aperture
FEM	Finite Element Method
PEEK	Polyether ether ketone
PET	Polyethylene terephthalate
PBS	Phosphate-buffered saline

Contents

1	Introduction	1
2	Biomedical Optics	2
2.1	Light propagation in tissue	2
2.2	Diffusion theory	2
2.3	Bioheat equation	3
2.4	Immunostimulating Interstitial Laser Thermotherapy	3
2.5	Laser probes	4
2.5.1	Bare end fiber	5
2.5.2	Radial fiber	6
3	Source model	7
3.1	Intensity distribution	7
3.1.1	Bare end fiber	7
3.1.2	Radial fiber	9
3.2	Light propagation model	10
3.3	Heat transfer model	11
3.3.1	Bare end fiber	11
3.3.2	Radial fiber	13
4	Results	15
4.1	Intensity distribution	15
4.1.1	Bare end fiber	15
4.1.2	Radial fiber	18
4.2	Light distribution	21
4.2.1	Bare end fiber	21
4.2.2	Radial fiber	22
4.3	Thermal distribution	23
4.3.1	Bare end fiber	23
4.3.2	Radial fiber	28
5	Discussion	36
6	Conclusions and Outlook	37
7	Acknowledgments	37
8	References	38

1 Introduction

The use of heat for tissue ablation have become fairly common these days and is used in a variety of forms. The aim when using heat for tumor ablation is to raise the tissue temperature to a degree above 50°C, this to utilize the increased sensitivity of the tissue [1].

One technique investigated for tumor ablation is called Immunostimulating Interstitial Laser Thermotherapy (imILT^{CLS}), and is also the one that this project is centered around. This technique has been developed by Clinical Laserthermia Systems (CLS) in Lund, based on Karl Göran Tranberg's research at Lunds University Hospital. CLS has recently started its clinical studies on this technique in Europe [2]. Immunostimulating Interstitial Laser Thermotherapy is a method for tumor ablation that uses heat to reach a given temperature in a specific tumor location. This procedure can activate an immune response towards the remaining cancer cells, and it is based on a technique called Interstitial Laser Thermotherapy [3]. This method is only one of many tumor ablation techniques that have been developed through out history. One other technique for tumor ablation is radiofrequency ablation which utilizes an alternating current to induce friction in the tissue which in turn produces heat. A third example of a tumour ablation technique is called microwave ablation where an antenna delivers an oscillating electromagnetic field into the tumor, and this field creates friction and heat due to that the water molecules oscillate with the field [4].

What these different tumor ablation methods aim to achieve is to develop a treatment with a predictable temperature distribution and an accurate destruction of the tumor sites [5]. This could be aided by simulating the procedure before treatment to see the heat distribution within the tissue depending on different parameters. Some of these parameters are, estimated time of the procedure, type of applicator, placement of the applicator and in the case of imILT^{CLS} the placement of the temperature probe relative to the applicator. The simulations can help to reduce animal testing down to the most promising parameters and also reduce the number of different prototypes that needs to be tested before finding the optimal solution. This will then reduce the cost of developing a new applicator or treatment, since the cost of animal testing will be reduced, as well as the cost of producing the prototypes needed to find the optimal solution. Simulating the problem is thus both ethically relevant and cost effective.

The aim of this project is to develop a source model of how heat is distributed in tissue for the method imILT^{CLS}. Starting with ray-tracing simulations of a realistic fiber model and then move on to add tissue simulations using diffusion theory in COMSOL Multiphysics and implementing the Bioheat equation. The results are to be experimentally verified by using the equipment and *ex vivo* measurement protocoll developed by CLS [2].

2 Biomedical Optics

In this section all relevant theory behind the project is presented. This theory is presented in the order so that it follows the three steps used in this project to develop a source model. The models behind the source model and thus the three steps are; Light propagation in tissue, Diffusion theory, Bioheat equation, imILT^{CLS} and Laser probes and are presented in the following subsections.

2.1 Light propagation in tissue

Biological tissue is often referred to as turbid media or highly scattering media and is optically inhomogeneous. Even though biological tissue is referred to as highly scattering, it is also an absorbing medium. In the wavelength range of 400 – 1350 nm biological tissue have a very low absorption relative to its scattering, often referred to as the optical window. The mean free path of a scattering event in this region is in the 0.1 mm range and for an absorption event it can be in the range of 10 – 100 mm [6]. This mean free path is defined as the reciprocal of either the scattering coefficient, μ_s , or absorption coefficient, μ_a . These coefficients describe the probability of either a scattering or absorption event per unit path length [7]. The absorption coefficient in biological tissue in the wavelength range of 400 – 1350 nm, is in the order of $\mu_a = 0.1 \text{ cm}^{-1}$ and the scattering coefficient in the order of $\mu_s = 100 \text{ cm}^{-1}$ [6].

For turbid media such as biological tissue a reduced scattering coefficient is used instead of the ordinary one, the two are connected by Equation 1. The variable connecting the two is called the anisotropy factor and is denoted g . This factor is given by the average cosine of the scattering angle and describes the direction of scattered light inside the medium. A value close to one of the factor g , as in biological tissues, means that the light is mostly forward scattered.

$$\mu'_s = \mu_s(g - 1) \quad (1)$$

2.2 Diffusion theory

One way of explaining light moving through a medium is by viewing the light as optical energy of a specific concentration. This optical energy then diminishes following a concentration gradient by means of diffusion [8]. The explanation above is one way of describing diffusion theory. Diffusion theory depends on that light has no preferred direction, which is said to be true after multiple scattering events. This means that diffusion theory is to be used when the absorption is low in respect to scattering in the propagation medium and when examining points a few scattering lengths away from a source, in biological tissue approximately 1 mm. The diffusion equation represented as a partial differential equation can be seen in Equation 2, where the parts on the left hand side represents a loss of photons and the one on the right a gain, i.e. a source [8], [9].

$$\frac{1}{c} \frac{\partial \phi(r, t)}{\partial t} - D \nabla^2 \phi(r, t) + \mu_a \phi(r, t) = S(r, t) \quad (2)$$

Where $D = \frac{1}{3(\mu_a + \mu'_s)}$ is the diffusion constant, also called the diffusion length, $\phi(r, t)$ is the fluence rate as a function of distance from the source and time, μ_a is the absorption coefficient and $S(r, t)$ is the source function.

In this project a stationary version of the diffusion equation is used because a continuous laser beam is utilized instead of a pulsed one. The assumption is then that directly after turning on the laser, a specific light distribution is generated. This results in the following equation [9]:

$$-D\nabla^2\phi(r) + \mu_a\phi(r) = S(r) \quad (3)$$

When solving this partial differential equation for a system consisting of varying parameters and complex boundaries, a numerical approach is desired. The numerical method used in this project is the Finite Element Method or FEM for short, which solves the equation for the whole system by dividing the problem into discrete arbitrary elements with associated equations. The solutions for each of the discrete elements are assembled into a larger system to calculate the solution for the whole problem [8].

2.3 Bioheat equation

Absorption of light will lead to an increase in temperature. This temperature increase and heat distribution is defined by Equation 4 below, called Pennes' equation, where on the left hand side, ρ is the density of the medium, c is the materials heat capacity, T is the temperature as a function of position and time and k is the thermal conductivity of the medium. On the right hand side of Equation 4 the first term represents the heat absorption due to blood perfusion, where ρ_b is the density of blood, c_b is the heat capacity of blood, ω_b is the blood perfusion rate and $T_b - T$ is the difference in temperature between the blood and the surrounding tissue. The second term on the right hand side represents the metabolic heat source and the third term represents an external heat source, in this case the heat generated by the absorption of light in the tissue [10]- [12].

$$\rho c \frac{\partial T}{\partial t} + \nabla(-k\nabla T) = \rho_b c_b \omega_b (T_b - T) + Q_{met} + Q_{ext} \quad (4)$$

2.4 Immunostimulating Interstitial Laser Thermotherapy

Immunostimulating interstitial laser thermotherapy, imILT^{CLS}, is a treatment method developed by CLS and is based on the tumor ablation technique, interstitial laser thermotherapy. The techniques are both based on the effect of temperature change on biological tissue.

When it comes to laser treatments the word thermotherapy is used to define a treatment temperature above 50°C. For the treatment investigated in this project, i.e. imILT^{CLS}, temperatures between 43°C and 50°C at the tumor border are aimed for. In this temperature interval three effects can be observed: direct cell death, vascular destruction within the tumor, and the increased sensitivity to heat of the tumor cells [1], [13]- [15]. Coagulation of tissue can be seen from temperatures above 45°C [16], [17]. Inside the tumor, both

coagulation and rapid cell death is achieved since the temperatures here are above 50°C, and if the temperatures are raised above the boiling temperature of water, i.e. 100°C, carbonisation can occur. The complete ablation of imILT^{CLS} cannot be seen directly after treatment since it continues for hours or days after the treatment period.

The procedure of imILT^{CLS} is to reach a temperature of 46°C at the tumor border and keep it there for approximately 30 minutes. This is done by turning the laser off above 46°C and on below this temperature. By doing so, an immunological response can be induced by delayed apoptosis and vascular damage [14]. The immunological response can take care of the remaining cancer cells at the tumor border and eventual metastasis.

2.5 Laser probes

To perform different kinds of treatments a safe and effective delivery system from the laser source to the treatment volume is needed, and one way to do this is to use optical fibers. The easiest form of an optical fiber consists of a core, a cladding and in most cases also a coating for extra protection of the fiber. Most of the fibers used for medical applications, where a high intensity is required, are so called multi-mode fibers, i.e. fibers permitting multiple ray-trajectories inside the core [1].

Optical fibers depend on total internal reflection which in turn depends on the difference in refractive index between core and cladding. The requirement for total internal reflection is that the angle of incidence, θ_a , on the fiber entrance relative to the optical axis is such that it fulfills the requirements of Equation 5 below. Where, NA is the numerical aperture, n_0 is the index of refraction of the material surrounding the entrance of the fiber, n_1 the index of refraction of the core and n_2 the index of refraction of the cladding. The angle θ_a can also be seen as the maximum output angle from the fiber, if the refractive index of the surrounding material is used at the exit as n_0 instead of the one at the entrance.

$$NA = n_0 \cdot \sin \theta_a = \sqrt{n_1^2 - n_2^2} \quad (5)$$

As seen from equation 5 the index of refraction of the cladding needs to be smaller than the one of the core for the relation to be fulfilled. This is often done by using for example silica for the core, which has a refractive index of approximately 1.45, and doped silica for the cladding. When doping silica the index of refraction is reduced, by a quantity which depends on the substance used in the doping process, and its concentration. [1].

The NA and acceptance angle can also be connected to the allowed release angle inside the fiber by Equation 6, where n_1 is the refractive index in the core and θ_r is the release angle relative to the optical axis.

$$n_0 \cdot \sin \theta_a = n_1 \cdot \sin \theta_r \quad (6)$$

Equations 7 to 9 show the equations used by COSMOL Multiphysics for the initial wave vector components which in turn is used to determine initial direction of the rays.

$$k_x = \frac{\omega n}{c} \cos \theta \sin \phi \quad (7)$$

$$k_y = \frac{\omega n}{c} \sin \theta \sin \phi \quad (8)$$

$$k_z = \frac{\omega n}{c} \cos \phi \quad (9)$$

Here ω is the angular frequency, θ is an angle determined by the decided release axis, and ϕ is an angle going from 0 to the release angle θ_r [18].

The ray tracing module in COMSOL Multiphysics uses the following equations to calculate direction and position of the released rays assuming a constant refractive index and non-absorbing media [18].

$$\frac{d\mathbf{k}}{dt} = 0 \quad (10)$$

$$\frac{d\mathbf{q}}{dt} = \frac{c|\mathbf{k}|}{n} \quad (11)$$

Where \mathbf{k} is the wave vector, t is the time, \mathbf{q} is the position vector, c is the speed of light and n is the refractive index in the medium [18].

2.5.1 Bare end fiber

One of the applicators used in this project is a so called bare end fiber. The fiber has a diameter of approximately 0.5 mm, consists of three layers and has a flat top profile. These three layers are core, cladding and coating. The core consists of pure silica or silica quartz and has a refractive index of approximately 1.45 and a diameter of 0.4 mm. Used for cladding in this fiber is fluorine doped silica with a refractive index of 1.44 and a thickness of 20 μm . The layer of coating is made of polyimide and has a refractive index of 1.7 and a thickness of 15 μm . The theoretical acceptance and divergence angle of this bare end fiber in air is $\theta_a = 12.7^\circ$ and its $NA = 0.22$. Its acceptance and divergence angle is shown as θ_a in Figure 1.

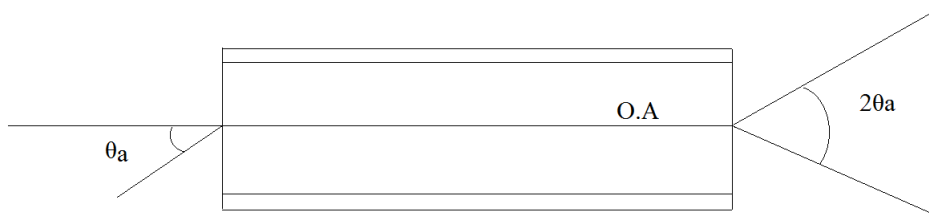


Figure 1: A schematic image of how the acceptance angle and divergence angle, θ_a , is defined.

2.5.2 Radial fiber

The other type of laser applicator, i.e. optical fiber, used for this project is the radial fiber. A radial fiber has an intensity profile like a disk with a specific divergence angle shown in Figure 2, in this case approximately $\theta_a = 15^\circ$. The radial fibers used in this project have two different sizes, fiber A has an outer diameter of 1.81 mm, and fiber B one of 1.16 mm. The materials of core and cladding are the same as for the bare end fiber and therefore the refractive index, NA, acceptance angle and release angle are the same. The outer diameters of core and cladding for fiber A is 0.60 mm and 0.72 mm respectively and for fiber B the corresponding values are, 0.550 mm and 0.605 mm respectively. The specific diameters of each fiber layer for the two fibers are presented in Table 1.

Table 1: Materials and their Outer Diameters (O.D.) for the different layers of the radial fibers.

Material	Layer	O.D. [μm]	
		Fiber A	Fiber B
Silica glass	Core	600	550
Fluorine doped silica	Cladding	720	605
Polyimide	Coating	760	640
Nylon	Buffer	1100	810
UV glue	In back of fiber	1200	860
PEEK	PEEK	1750	1150
PET	Tubing	1810	1210
Air	Air in cap	770	640
UV glue	Glue in cap	770	640
Silica glass	Cap	1750	1150

The most significant difference in construction between a bare end fiber and a radial fiber is the number of layers, and the end of the radial fiber core which consists of a cone with a protective closed capillary around it. The bare end fiber has a flat top profile and no protective cap. An image of a 2D model of a radial fiber modeled in COMSOL Multiphysics is shown in Figure 2 below.

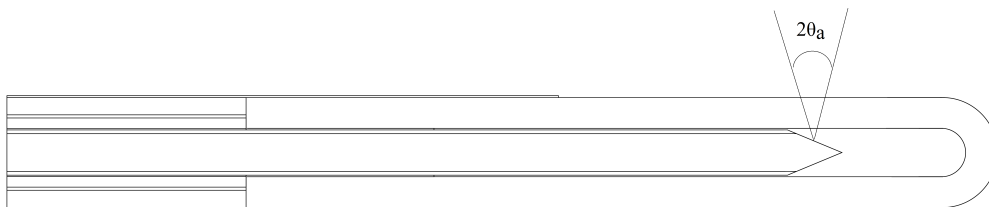


Figure 2: A 2D drawing of a radial fiber, which shows the different layers and the structure of the fiber. The image also shows the definition of the divergence angle, θ_a .

3 Source model

This section is about how the source model is built up step by step for the fibers and also about the different validation experiments made to support the models. The three steps taken to develop the source model are, implementation of the intensity distribution model in the fiber, the light distribution model in the tissue and the thermal distribution model in the tissue. These three steps are explained in the following subsections respectively. After finishing each step, a validation is made, if possible. Validations are made for the intensity distribution model and the heat distribution model, but not for the light distribution model since it would be very difficult and time consuming.

3.1 Intensity distribution

The intensity distribution of two different fibers, bare end and radial, are simulated and experimentally validated to develop a model of the intensity distribution. This section explains the method behind the simulations as well as the validation experiments for the two different fiber types.

3.1.1 Bare end fiber

Simulation

Simulating ray tracing and intensity distribution of a fiber starts with building the correct geometry. The geometry for the bare end fiber is modeled by making a 2D drawing in COMSOL Multiphysics corresponding to the half longitudinal section, and revolve it 360° around the fiber axis. In this case the 2D drawing consists of three rectangles with widths corresponding to the column called layer thickness specified in Table 2. Each layer in the fiber is assigned a material with different refractive index, which also can be seen in Table 2.

Table 2: Parameters for the different layers of the bare end fiber.

Material	n	Layer	Layer thickness [μm]	Reference
Silica glass	1.499	Core	200	[19]
Fluorine doped silica	1.4331	Cladding	20	[19]
Polyimide	1.7	Coating	15	[20]

After creating the described geometry the release of rays inside the fiber is specified using the "Release from grid" feature in COMSOL with a conical shape. The half angle of the release cone corresponds to the maximum release angle, θ_r , inside the fiber calculated from Equation 6.

Experiments

The following experiment was performed to be used as validation of the theoretical illumination model developed in COMSOL Multphysics for the bare end fiber. Validation of the intensity profile of the bare end fiber was made by placing a paper screen at three different distances perpendicular to the fiber axis, this to visualize the beam released by the fiber. The different distances from the fiber tip used for the experiments were 20 mm, 40 mm and 80 mm. Images were taken of the intensity profiles in a plane perpendicular to the axis of the light distribution, as seen in Figure 3.



Figure 3: Here the set up used for the validations of the bare end fiber is shown. The red marking on the paper screen is used to focus in the right plane.

To validate the results from the intensity distribution simulation for the bare end fiber, the angle at which light exits the fiber in the simulation is compared to that of the experiments. This validation is done by determining the divergence angle in the simulations as well as in the experiments.

The calculation of the angle in the simulation is made by creating a Poincaré map placed perpendicularly to the fiber axis at a distance of 4 cm from the fiber exit and evaluating its radius. These values are then to be used in Equation 12 as, x and y , respectively. The equation gives the divergence angle of the fiber where x is the separation and y is the intensity radius.

Calculation of the divergence angle from the experiment is made by evaluating the intensity along a line through the center of the the intensity pattern and in that way determining the diameters and radii of the intensity profiles at the three different distances. The different radii are then plotted against the different distances and a linear fit is calculated. From the linear fit the divergence angle can be calculated by using the radii as y in Equation 12 and the distances as x .

$$\theta_a = \tan^{-1} \left(\frac{y}{x} \right) \quad (12)$$

3.1.2 Radial fiber

The intensity model simulation is developed in the same way for both fiber A and B, but the validation experiment is only done for fiber A. This since the fibers are identical in their construction but have different thickness, which in turn means that the divergence angle in air is the same for both fibers and it is thus enough to only validate the divergence angle for one of them.

Simulation

Ray tracing and intensity distribution simulations for a radial fiber begin with a realistic geometrical model of such a fiber. The geometry of the radial fibers used in this project was achieved by creating a 2D drawing in COMSOL Multiphysics corresponding to the half longitudinal section revolved around the fiber axis for 360° . The 2D drawing is the same as in Figure 2 but cut in half along the rotational axis and is thus built up of different combined geometrical shapes. Each layer is assigned a specific material with specific material properties, such as refractive index. The parameters for the different layers in the fibers are described in Table 3. Note that the thicknesses of the coating layer and the buffer layer do not match the defined outer diameters in Table 1. This is due to the fact that the simulation program used has problems when the thin layers in the back and front of fiber do not match. Since the most important parts for the evaluation of the fibers for this project are in the part by the cap, the coating layer is changed in the simulation to match the layer of glue in the cap. This also results in reducing the buffer layer the same amount that the coating is enlarged. In Table 3 the tubing layer is missing, which is due to that this layer is not used for the simulations. The reason for this is that it caused complications that there was no time to resolve during this project. These changes are acceptable since they do not affect the aspects to be evaluated.

Table 3: Parameters for the different layers of the simulated radial fibers.

Material	n	Layer	Layer thickness [μm]		Reference
			Fiber A	Fiber B	
Silica glass	1.499	Core	300	275	[19]
Fluorine doped silica	1.4331	Cladding	60	27.5	
Polyimide	1.7	Coating	25	17.5	[20]
Nylon	1.53	Buffer	170	85	[21]
UV glue	1.56	In back of fiber	50	25	[22]
PEEK	1.67	PEEK	275	145	[23]
Air	1.0	Air in cap	25-385	17.5-320	
UV glue	1.56	Glue in cap	25	17.5	[22]
Silica glass	1.499	Cap	490	255	[19]

As for the bare end fiber the release of rays inside the fiber is specified by using the "Release from grid" feature in COMSOL Multiphysics. In this case, as in the case of the bare end fiber, a release feature with a conical shape is used with the half release cone angle corresponding to the maximum release angle inside the fiber, i.e. θ_r .

Experiments

The validation of the intensity profile of a radial fiber was performed by building cylinders of thin white paper, and placing them around the fiber with the axis parallel and centered to the fiber axis. Cylinders of three different diameters, 16 mm, 20 mm and 40 mm, were built. Figure 4 below shows the set up used for the validation experiments of the radial fiber. As for the bare end fiber, images were taken for analysis in a plane perpendicular to the emission plane.

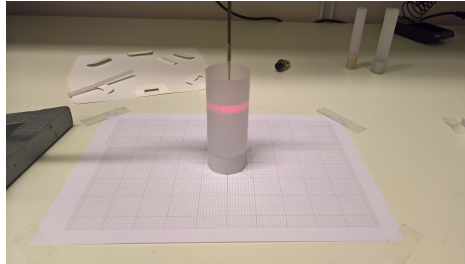


Figure 4: The set up used for the validations of the intensity distribution of the radial fiber.

Validation of the results from the intensity distribution simulations for the radial fiber is done by comparing the divergence angle of the fiber in the simulation to the one of the experiments for fiber A.

The calculation of the angle in the simulation is made by creating a Poincaré map placed parallel to the fiber at a distance of 1 cm from the wall of the fiber cap and evaluating its width. These values are then to be used in Equation 12 as, x and $2y$, respectively.

To analyze this angle for the experiments the half height of the ring seen in Figure 4 is used together with the distance between fiber and cylinder. These variables are plotted against each other and a linear fit is calculated. As for the bare end fiber the divergence angle can be calculated by using the y -value from the linear fit as y and the x -value as x in Equation 12. The analysis of the images is done using MatLab by evaluating the intensity of a line parallel to the fiber axis centered on the cylinder.

3.2 Light propagation model

The simulation of light distribution in tissue is performed using diffusion theory, more specifically a stationary Helmholtz equation. Calculations made in the simulations are only done for the tissue domain, i.e. not for the fiber domains. This is done since the diffusion would be incorrect in the fiber domains because of the negligible scattering in them. The source term used is extracted from the ray tracing simulations as the intensity of the surface where the light exits the fiber. For the bare end fiber the source is defined as the intensity of the flat end surface, and for the radial fiber it is instead defined as the surface of the glass cap at the end of the fiber. This source term represents an external light source and is a part of the term $S(r)$ in Equation 3.

Table 4: Parameters for Bovine cardiac muscle.

Parameter	Parameter value	Reference
n	1.41	[25]
g	0.965	[26]
μ_s [1/m]	14 000	[26]
μ'_s [1/m]	490	[26]
μ_a [1/m]	30	[26]

The parameters used for absorption and scattering in the simulations are representing those of bovine cardiac muscle since that is the tissue type used for the validation experiments. A list of the used parameters and their respective reference is presented in Table 4.

3.3 Heat transfer model

This section describes the process of developing the heat transfer simulations as well as the validation experiments, for the two fibers types, bare end and radial respectively. The heat distribution model is developed by using the Bioheat equation, Equation 4, with the blood perfusion term, $\rho_b c_b \omega_b (T_b - T)$, and metabolic heat source term, Q_{met} , equal to zero. This since the simulation and the validation experiments are done *ex vivo*. In COMSOL Multiphysics this is done by using the Bioheat transfer module. The validation of this part is done using the laser system developed by CLS and their protocol for *ex vivo* measurements. The heat parameters used for bovine muscle in the simulations are presented in the table below.

Table 5: Heat parameters for Bovine cardiac muscle.

Parameter	Parameter value	Reference
c [J/kg · K]	3430	[27]
k [W/m · K]	0.418	[28]
ρ [kg/m ³]	1016	[29]

3.3.1 Bare end fiber

Simulation

The heat transfer simulation for the bare end fiber is developed by using the results from the light distribution model as an external heat source corresponding to the term, Q_{ext} in Equation 4. This is done by multiplying the fluence rate received from the Helmholtz equation with the absorption coefficient. The heat parameters used for this fiber model is presented in Table 6 below.

Table 6: Heat parameters for the bare end fiber.

Material	c [$J/kg \cdot K$]	k [$W/m \cdot K$]	ρ [kg/m^3]	Reference
Silica glass	703	1.38	2203	[31], [30]
Fluorine doped silica	703	1.38	2203	
Polyimide	1090	0.12	1420	[20]

To simulate an imILT^{CLS} treatment a step function needs to be added, that becomes zero at the target temperature of 46°C and goes to one when below the target temperature. This step function is added to simulate the ON-OFF behavior of the laser during a treatment. To measure the temperature for the step function a domain point probe is added at a distance of 5 mm perpendicular to the fiber axis and 2 mm in front of the fiber due to its forward directed light, which can be seen as point 1 in Figure 5. The temperature is also measured at three other points using the domain point probe function. These are in the core, in the cladding and in the coating all at the fiber tip, and can be seen as points 2, 3 and 4 in Figure 5, respectively. The wavelength and power used for the simulations are 1064 nm and 1 W respectively.

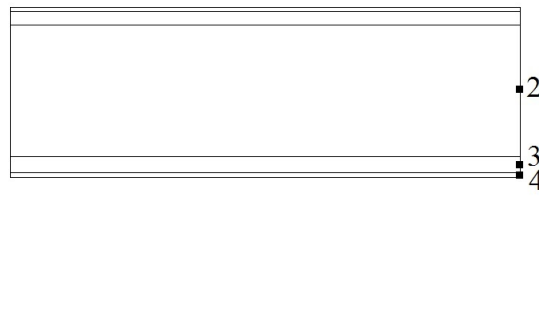


Figure 5: A schematic image of a bare end fiber and the four points at where the temperature is measured in the simulation of the fiber. 1: In the tissue 5 mm away from the fiber. 2: In the core by the fiber tip. 3: At the fiber tip in the cladding. 4: In the coating layer at the fiber tip.

Experiment

The validation experiments of the heat distribution model for the bare end fiber is done by placing bovine cardiac muscle in a Phosphate-buffered saline (PBS) solution and place it in a water bath. The water bath is used to heat up the tissue to a temperature of 37°C and keep it at that temperature throughout the experiment. When the temperature of the tissue is approximately 37°C a template with holes spaced 5 mm from each other is placed on top of the tissue and the fiber and temperature probe are inserted. The fiber is placed at a distance of 5 mm from the temperature probe and at a depth inside the tissue of 17 mm. The temperature probe is placed a few millimeters deeper than the fiber since the bare end fiber is radiating in the forward direction. After placement of fiber and temperature probe the treatment is started, first there is a warm up time, which is the time it takes for the laser to heat up the tissue to 46°C at the temperature probe position. Then there is a

treatment time of 30 minutes where the temperature is kept at 46°C by turning the laser off and on. After finishing the treatment the tissue is divided along the plane of the fiber and temperature probe, and the lesion is measured using a ruler. The wavelength used for the experiments is 1064 nm and the power used is 1 W.

3.3.2 Radial fiber

The simulations of this fiber model is done in two ways for fiber A, and in one way for fiber B. The first one is to simulate an imILT^{CLS} treatment, meaning having the laser turn on and off at a specific temperature, this is only done for fiber A. The other one is to keep the laser on for a specific time corresponding to the time it takes to detect smoke or a burnt scent when keeping the laser at a constant power in the experimental part. The second way of simulating heat distribution is done for both the radial fibers, and is further on referred to as the Burn simulations and Burn experiments. These burn trials are made to detect differences between two fibers with the same construction but different thicknesses.

Simulation

When developing the heat transfer simulation for the radial fiber, the results from the light distribution model simulation is used as an external heat source corresponding to, Q_{ext} in Equation 4. This is done by multiplying the fluence rate received from the Helmholtz equation with the absorption coefficient of the tissue. The heat parameters used for this fiber is show in Table 7 below. In Table 7 the heat capacity and thermal conductivity for the UV glue is assumed to be the same as for Nylon. The reason for this is that these parameters for the glue could not be found and the properties of Nylon were those assumed closest and were thus used.

Table 7: Heat parameters for the different materials of the radial fiber.

Material	$c [J/kg \cdot K]$	$k [W/m \cdot K]$	$\rho [kg/m^3]$	Reference
Silica glass	703	1.38	2203	[31], [30]
Fluorine doped silica	703	1.38	2203	
Polyimide	1090	0.12	1420	[20]
Nylon	1700	0.25	1150	[32]- [34]
UV glue	1700	0.25	1050	[32], [33], [35]
PEEK	320	0.25	1310	[36], [37]
PET	439.3	0.3	1350	[38], [24]
Air	1005	0.0257	1.205	[39], [40]

To measure the temperature at different points in the fiber and tissue, domain point probes are added in COMSOL Multiphysics. The measurement points for the radial fiber are; in the glass cap parallel to the radiation point, in the lower edge of the UV glue inside the glass cap, and in the tissue at a distance of 10 mm from the radiation point. These three points can be seen in Figure 6.

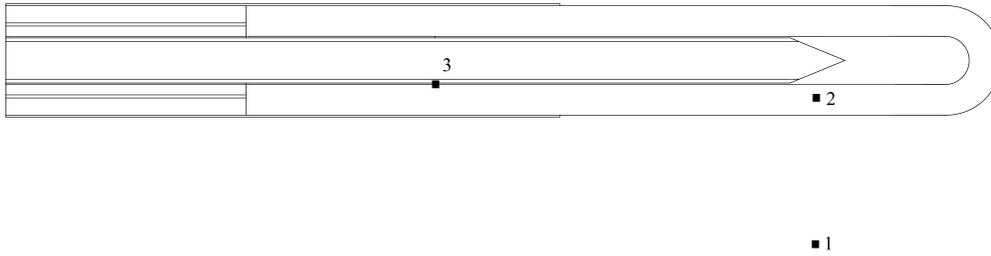


Figure 6: A schematic image of a radial fiber and the three points at where the temperature is measured in the simulations of the radial fibers. 1: In the tissue 10 mm away from the fiber. 2: In the glass cap by the core tip. and 3: At the end of the glue layer closest to the fiber tip.

For the simulation, where an imILT^{CLS} treatment is to be recreated, an ON-OFF behavior is added with the help of a step function and the domain point probe placed in the tissue. This step function goes to zero when the target temperature of 46°C is reached at the measuring point, and to one, when below this temperature. The step function is then multiplied with the heat source, meaning that the heat source is turned ON and OFF depending on the temperature at the measuring point. The simulation time for the treatment is first put to 30 minutes plus the time it takes to reach 46°C the first time but is changed to 20 minutes due to memory errors on the computer used for the simulations. The results from the last 10 minutes of a 30 minute treatment is only seen *in vivo* and not *ex vivo*, so the validation using experimental *ex vivo* data for 30 minutes can still be made.

The Burn simulations, developed for both fiber A and B are done in the same way except for the ON-OFF regulation achieved using the step function. Instead the laser is kept on for a specified amount of time corresponding to that of the results in the experimental part. The evaluation of the burn simulations are only made on the temperatures in the glass cap and in the glue and not on the temperatures in the tissue. This since the part aimed to investigate with these simulations is the damage inflicted on the fibers and not the tissue.

Experiment

Validation of the heat distribution model simulations for the radial fibers, is done by placing bovine cardiac muscle in a PBS solution and place it in a water bath. As in the case for the bare end fiber validation experiment, the water bath is used to heat up the tissue to a temperature of 37°C and keep it at that temperature throughout the experiment. After reaching the wanted start temperature of 37°C a template with holes spaced 5 mm from each other is placed on top of the bovine cardiac muscle tissue and the fiber and temperature probe are inserted. The fiber is centered on the tissue at a depth of 28 mm placed 10 mm away from the temperature probe also placed at a depth of 28 mm. After placement of fiber and temperature probe the laser is turned on, which in turn starts the heating process.

For the validation of the heat distribution model for radial fiber A, the treatment corresponding to an imILT^{CLS} , there is first a warm up time after turning on the laser. This warm up time corresponds to the time it takes for the laser to heat up the tissue at the

temperature probe position to a temperature of 46°C. Then there is a treatment time of 30 minutes where the temperature is kept at 46°C by turning the laser off and on. After finishing the treatment the tissue is opened up along the plane of the fiber and temperature probe, and the lesion is measured using a ruler.

When doing the experiments for the burn simulations the set up used is the same but the laser is instead kept on constantly until smoke or a burnt scent coming from the tissue is detected. The evaluation of these experiments are only done by comparing the time it takes to burn the respective fiber.

4 Results

In this section the results from the developed model and the validation experiments are presented. The results are presented in three different subsections corresponding to the three different steps taken to develop the source model.

4.1 Intensity distribution

This part of the result section is focused on the intensity distribution results from both fibers. The results are presented for both the simulations and the experiments.

4.1.1 Bare end fiber

The results from the ray tracing simulations and thus the intensity distribution for the bare end fiber is shown in the following figures. Figure 7, shows the ray trajectories through a bare end fiber and also the intensity distribution after exiting into air. The light exiting the fiber has a conical shape as expected for this fiber type.

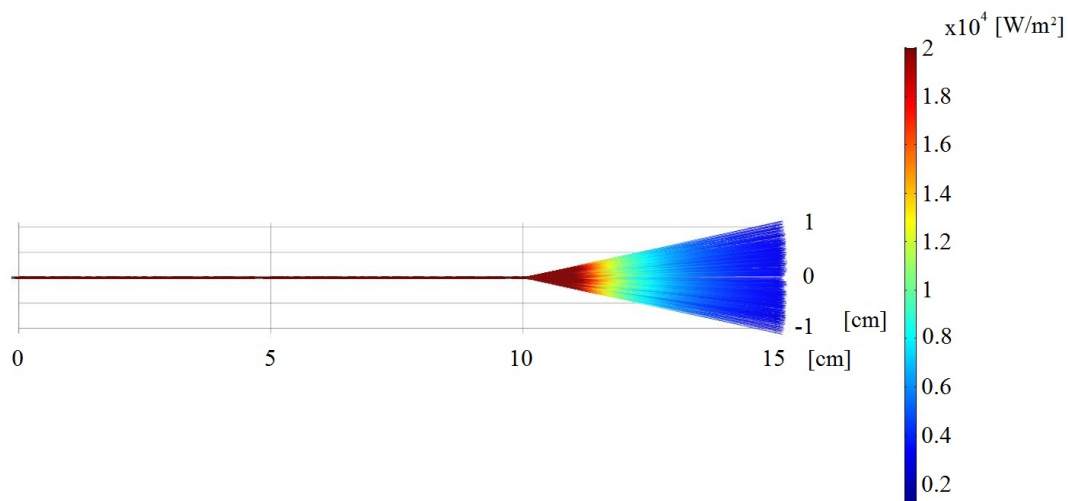


Figure 7: Simulation results showing the intensity distribution and ray tracing of the bare end fiber. The colorbar represents the intensity.

Figure 8 shows the Poincaré map produced in COMSOL Multiphysics for the ray tracing simulation of the bare end fiber. Evaluation of the distribution angle in air from this figure gives a divergence angle, $\theta_a = 12.68^\circ$ calculated from Equation 12 where $y = 9$ mm is the radius of the Poincaré map and $x = 40$ mm is the distance from the end of the fiber to the evaluation plan.

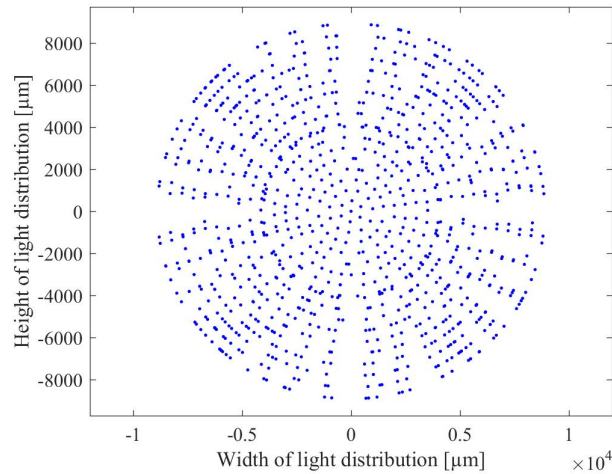


Figure 8: Poincaré map 4 cm away from the fiber tip, centered at the fiber axis.

The results from the validation experiments are presented below. Figure 9 shows the intensity of the fiber output at different distances from the screen versus number of pixels.

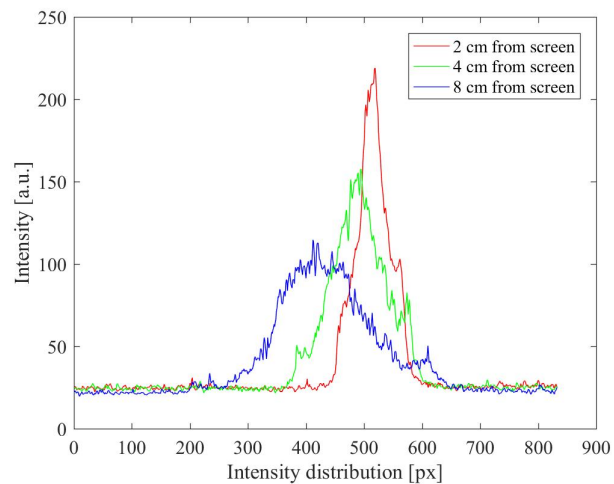


Figure 9: Intensity distribution of the bare end fiber at three different distances from the screen. The right curve (red) represents a distance of $x = 2$ cm, the middle one (green) a distance of $x = 4$ cm and the left one (blue) a distance of $x = 8$ cm.

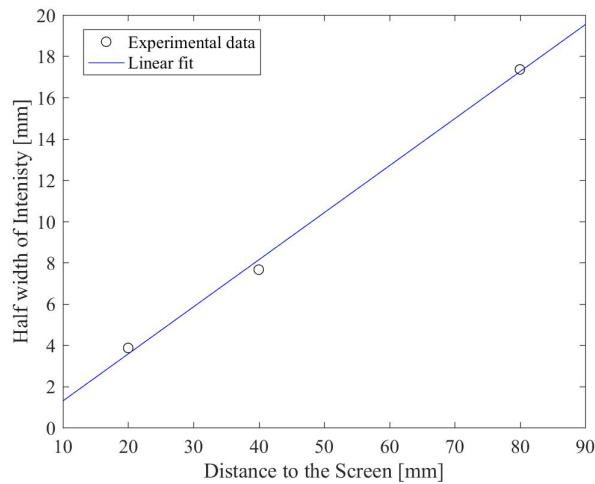


Figure 10: A linear fit for three data points (circles) representing the half width of the intensity distribution at the three distances between fiber and screen.

Figure 10 shows a linear fit of the half width of the intensity distribution versus the distance to the screen. The equation of the linear fit is:

$$y = 0.228x - 0.99 \quad (13)$$

This gives an experimental divergence angle in air of $\theta_a = 12.84^\circ$ for the bare end fiber. The divergence angle for the bare end fiber in air, both for the simulation and validation experiment, is close to the one calculated from the numerical aperture. For the simulation the divergence angle is the same as the one calculated from the NA, meaning that the ray tracing simulation of the bare end fiber agrees with the theory. The divergence angle for the experiments is larger than the one calculated from Equation 6, the reason is most likely flaws in the experiment, but could also be due to tolerances during fiber production. One possible reason for the larger angle is the the paper screen that was built may have tilted a bit forward causing the seen intensity distribution to be enlarged, thus causing the evaluated angle to be enlarged as well. Another possible reason for an enlarged angle is that the paper used in the experiments scatters the light which enlarges the light distribution on the screen. The evaluation for the experiment could also have affected the result, this since the decision of where to measure the width of the intensity distributions in Figure 9 is made manually.

4.1.2 Radial fiber

The next two figures, i.e. Figure 11 and 12 show the ray tracing results and a Poincaré map for radial fiber A respectively.

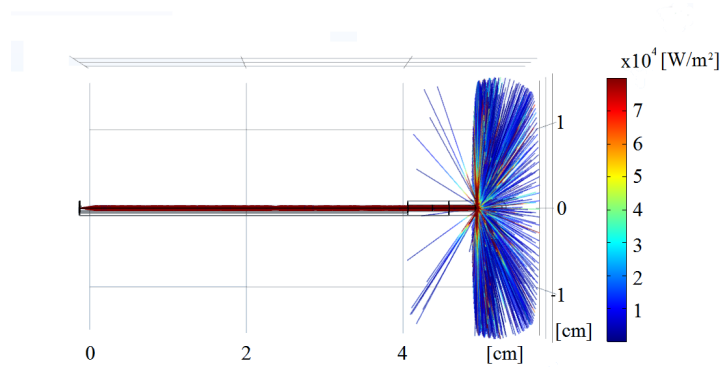


Figure 11: Simulated intensity distribution and ray tracing results of the investigated, radial fiber A.

Figure 11 shows an image of the ray tracing results for radial fiber A, i.e. the rays trajectories in the fiber and the intensity distribution after exiting. The figure below, Figure 12, shows the Poincaré map for the ray tracing simulation of radial fiber A. Evaluation of the distribution angle in air from this figure gives a divergence angle of, $\theta_a = 14.0^\circ$ calculated from Equation 12, where $y = 2.5 \text{ mm}$ is the half width of the Poincaré map in zero and $x = 10 \text{ mm}$ is the distance from the radial fiber to the plane at which the evaluation takes place.

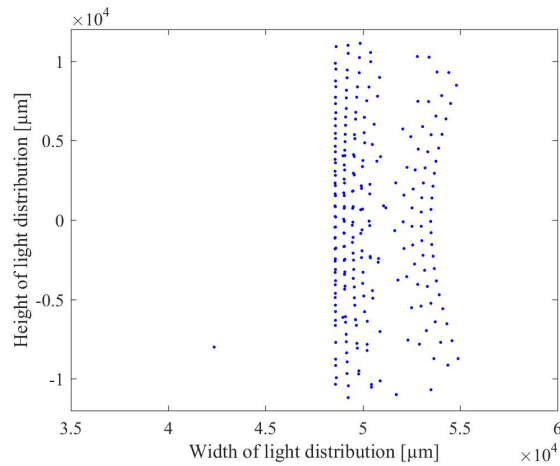


Figure 12: A Poincaré map parallel to the fiber axis direction, 1 cm away from the fiber.

Figure 13 and 14 presents the ray tracing results and a Poincaré map for fiber B respectively. The first one displays the rays inside the fiber and when released into air, as well as the intensity expressed as a color bar.

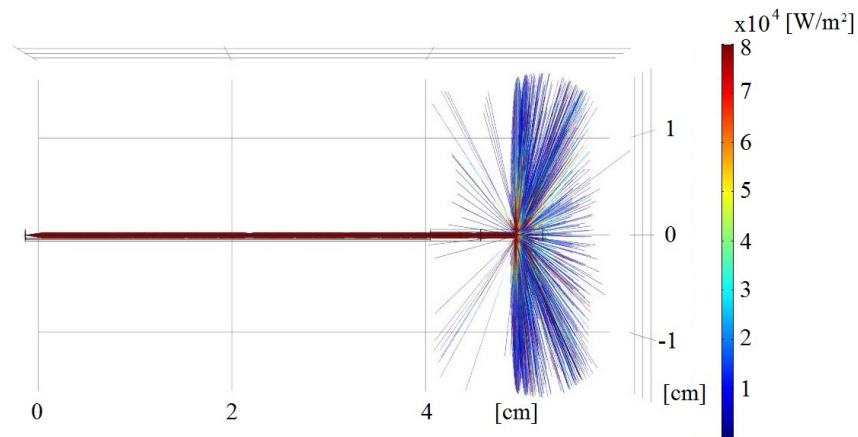


Figure 13: Simulation results showing the intensity distribution and ray tracing results of the investigated, radial fiber B.

The divergence angle obtained from the simulation is $\theta_a = 14.0^\circ$ and can be determined from Figure 14, which shows a Poincaré map placed parallel to the fiber. The angle is calculated from Equation 12, where $y = 2.5$ mm is the half width of the Poincaré map and $x = 10$ mm is the distance from the radial fiber to the evaluation plane.

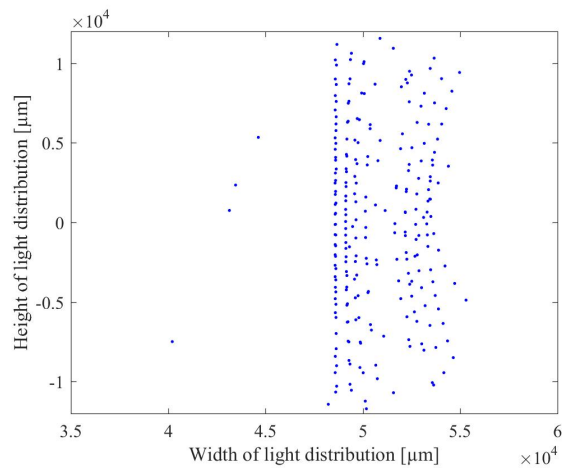


Figure 14: A Poincaré map for fiber B parallel to the fiber axis direction, 1 cm away from the fiber.

Figure 15 below shows the intensity distribution of the radial fiber for three different cylinder diameters, 16 mm (green), 20 mm (blue) and 40 mm (red).

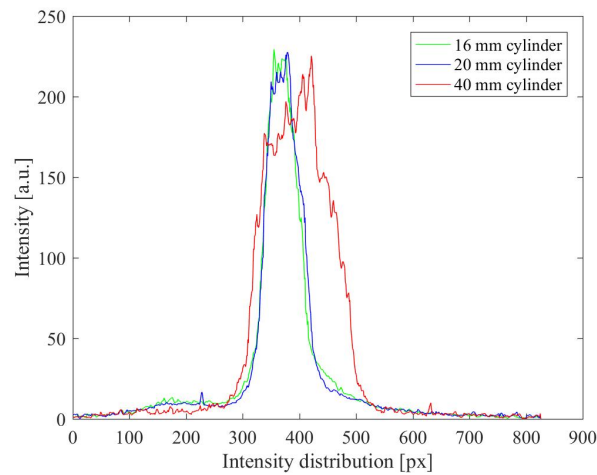


Figure 15: The intensity distribution of the radial fiber at three different distances to the cylinder walls. The right one (red) represents a distance of 20 mm between fiber and cylinder, the middle one (blue) a distance of 10 mm and the left one (green) a distance of 8 mm.

From these intensities the half width could be determined for each distance and a linear fit could be calculated. This linear fit is shown in Figure 16. The equation of the linear fit is represented as equation 14 below.

$$y = 0.299x + 0.555 \quad (14)$$

This gives an experimental divergence angle in air of $\theta_d = 16.65^\circ$ for the radial fiber.

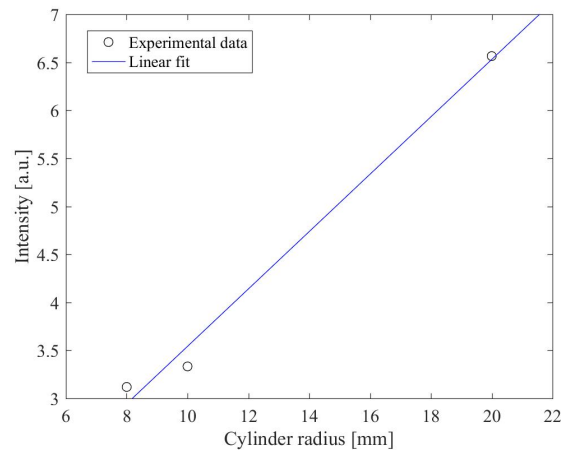


Figure 16: A linear fit for three data points representing the half width of the intensity distribution for the radial fiber at the three distances between fiber and cylinder wall, i.e. 8 mm, 10 mm and 20 mm.

For the radial fiber, the divergence angle calculated from the simulation and experiment respectively does not correspond as well to the given one, as the bare end fiber does to that calculated from the NA. The reason for this is that there are more parameters that can cause errors both in the simulation and in the experiment. For the simulation the divergence angle in air is 14.0° , which is 1° smaller than the given value of 15° . This error is

most likely caused by a discrepancy between the angle used for the simulations and the one of the fiber sample used for the measurements due to tolerances in the manufacturing process. This angle would cause differences in the divergence angle since rays inside the fiber cores are met with a different plane of incidence at the core tip boundaries depending on this angle. Another thing that could cause an error is how the evaluation of the diameters from the Poincaré maps in Figures 12 and 14 are made. The experiment for the radial fibers gave a divergence angle in air of 16.65° which is 1.65° larger than the given value. This error can be due to that the cylinders were made by hand and may thus not be perfectly cylindrical, which would cause the distance from fiber to cylinder wall to be different from the expected one. Other possible reasons for the errors are, that the fiber was not perfectly perpendicular to the table plane during the measurements, it was hard to place the fiber exactly in the middle of the cylinder and that the paper scattered the light. The result from these possibilities can either be that the height of the radiation pattern is reduced or enlarged, giving a smaller or larger divergence angle.

4.2 Light distribution

In the following sections the results from the light distribution model simulations are shown. The first section shows the result for the bare end fiber, and the second, shows the results for the radial fibers. This part is not validated directly as stated before, but is still presented in the results since the light distribution is connected to the heat distribution, which in turn is validated.

4.2.1 Bare end fiber

Figure 17 shows the results from the light distribution model simulations when simulating a laser source of 1064 nm with a power of 1 W. The result is displayed as the logarithmic of the values calculated from the Helmholtz equation in COMSOL Multiphysics. From the image it is seen that the distribution in a homogeneous medium is symmetrical. This is an expected result since the normal procedure to simulate diffuse light propagation from a bare end fiber is by placing a point source some small distance from the fiber tip, leading to an isotropic photon distribution in the medium.

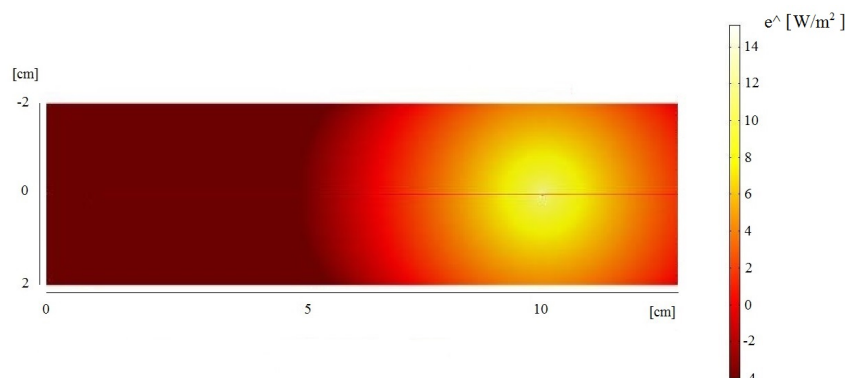


Figure 17: The light distribution of a bare end fiber, simulated using a laser wavelength of 1064 nm and a power of 1 W. Results from the simulation is presented as the logarithmic of the values calculated from the Helmholtz equation in COMSOL Multiphysics.

4.2.2 Radial fiber

This section is divided into two parts, one for the light distribution simulation of fiber A, and one for fiber B. Both simulation results are shown for a laser source of 1064 nm with a power of 8 W.

Simulation for fiber A

The result for the light distribution simulation for fiber A is shown in Figure 18.

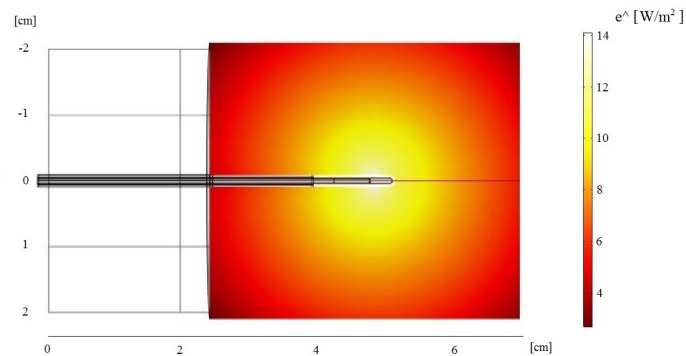


Figure 18: Light distribution of radial fiber A, simulated using a laser wavelength of 1064 nm and a power of 8 W. The results from the simulation is presented as the logarithmic of the values calculated from the Helmholtz equation in COMSOL Multiphysics.

Simulation for fiber B

Figure 19 shows the results from the light distribution model simulation for radial fiber B.

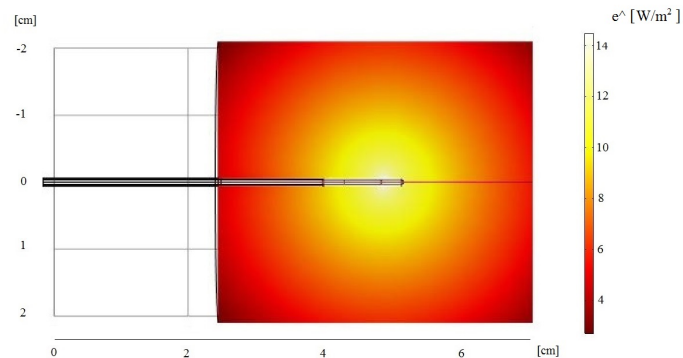


Figure 19: The light distribution of radial fiber B, simulated using a laser wavelength of 1064 nm and a power of 8 W. Results from the simulation is presented as the logarithmic of the values calculated from the Helmholtz equation in COMSOL Multiphysics.

For the two radial fibers a symmetrical distribution is also seen, here the intensity is higher than for the bare end fiber, which is due to the higher power used for the radial fibers.

4.3 Thermal distribution

The results from the heat distribution simulations of the two fiber types are shown in the following sections. First the results for the bare end fiber are presented and then results for the two radial fibers.

4.3.1 Bare end fiber

In this section the results from the heat distribution simulation and validation experiments for the bare end fiber are presented. All the results correspond to a treatment time of 30 minutes plus a warm up time, this using a laser power of 1 W and a wavelength of 1064 nm. Figures 20- 22 show the results from the heat distribution simulation of the tissue for the bare end fiber and can be compared to those of the corresponding validation experiment, i.e. Figures 23 and 24. The first image show a slice of the heat distribution in the tissue and fiber.

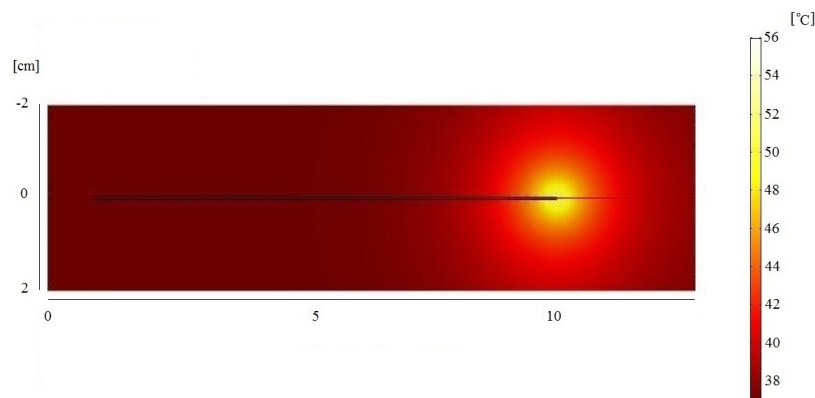


Figure 20: The heat distribution of the bare end fiber at a wavelength of 1064 nm, a power of 1 W and a treatment time of 30 minutes plus the warm up time of 3 minutes and 54 seconds. The colorbar represents the different temperatures in the image expressed in °C.

The graph corresponding to the left y-axis in Figure 21 represents the temperature in the tissue 5 mm away from the fiber axis and 2 mm in front of the fiber for approximately half of the total treatment time of 30 minutes plus a warm up time of 3 minutes and 54 seconds. This when simulating a source of 1 W that is turned off when reaching the target temperature of 46°C and on when below this temperature. The part corresponding to the right y-axis (red) in Figure 21 shows the power as a function of time for approximately half of the simulated treatment time, and here the ON-OFF behavior of the source due to the added step function in the heat source term is seen. This image is compared to Figure 24, corresponding to the temperature and power during one of the experiments.

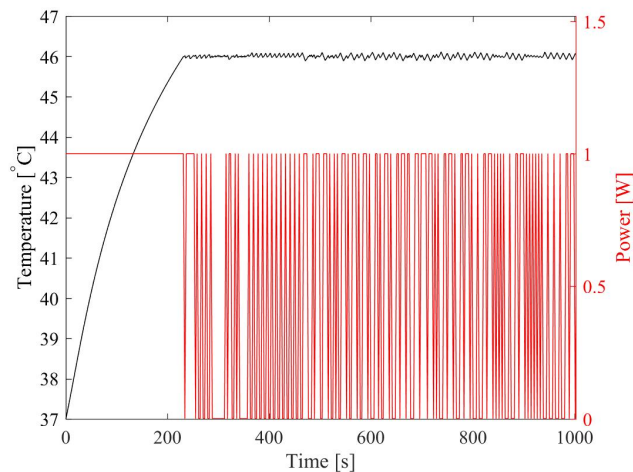


Figure 21: Left y-axis: The temperature as a function of time in the tissue at a distance of 5 mm from the fiber. This graph shows the temperature for approximately half of the total treatment time of 30 minutes plus a warm up time of 3 minutes and 54 seconds, when using a laser source of 1064 nm and 1 W. Right y-axis: Part of the power graph as function of time, received during a simulation of a treatment time of 30 minutes. The graph corresponds to the temperature graph in the figure.

Figure 22 shows the temperature simulated along a line perpendicular to the fiber axis, from the center of the fiber tip and a few millimeters out in the tissue. The dashed graph shows the temperature in the last time step of the heat distribution simulation, which is 33 minutes and 54 seconds and the solid corresponds to the temperature after the warm up time of 3 minutes and 54 seconds. These different temperatures are compared with the tissue damage in Figure 23 below.

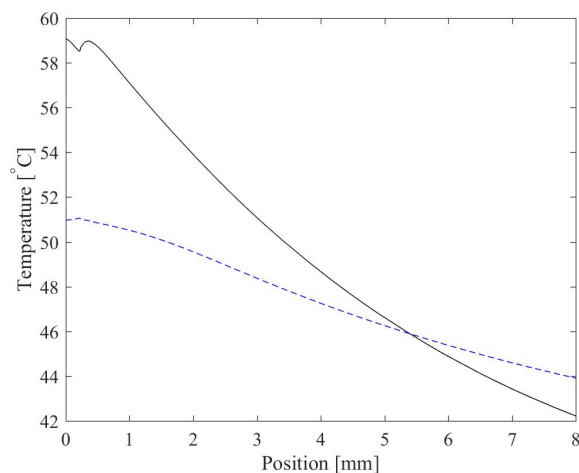


Figure 22: The temperature simulated at the fiber tip, from the center of the fiber and a few millimeters out in the tissue. These graphs corresponds to the temperature after 33 minutes and 54 seconds (dashed), and 3 minutes and 54 seconds (solid) from the beginning of the simulation time, when using a source of 1 W and 1064 nm.

One example of what the tissue may look like in the plane of the fiber after a treatment time of 30 minutes plus a warm up time of between 4 and 6 minutes is presented in Figure 23. The image also shows an example of the placement of fiber and temperature probe during a treatment, which is represented by the two metal cylinders, where the left one represents the temperature probe and the right one, the fiber.

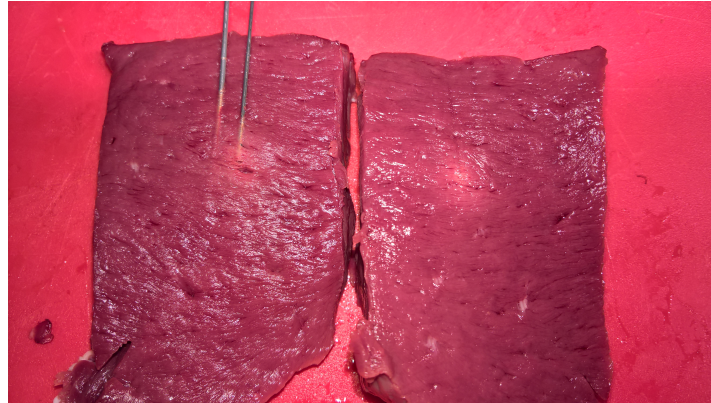


Figure 23: The result of a validation experiment using a bare end fiber and a source of 1 W and 1064 nm for 30 minutes plus warm up time. The two metal cylinders represents approximately where the fiber (right) and temperature probe (left) were placed and the distance between them is 5 mm. The slightly brighter part of the tissue is the area of the lesion.

The evaluation of the validation experiments made is gathered in Table 8, where $T_{Initial}$ corresponds to the initial temperature of the tissue, t_{warmup} is the warm up time, $t_{treatment}$ is the treatment time and d_{lesion} is the diameter of the lesion.

Table 8: Results from the experiments using the bare end fiber with a source of 1 W.

$T_{Initial}$ [°C]	t_{warmup} [min:sec]	$t_{treatment}$ [min:sec]	d_{lesion} [mm]
37.0	6:18	30:00	7.0
37.6	5:22	30:00	8.0
37.6	4:36	30:00 + 3:48	7.5

The lesion diameters presented here in Table 8 represents those seen in the lab when doing validation experiments corresponding to a treatment of approximately 30 minutes. If compared to the dashed graph in Figure 22, the temperatures in that area should be between 51 and 47°C after a treatment time of 30 minutes, which is not unlikely since the temperature of coagulation starts around 45°C depending on the time spent at that temperature. However, for *ex vivo* measurements most of the visible damage is caused during the warm up time and directly after it. The temperatures received from the simulation after the warm up time is shown as the solid graph in Figure 22 and there it can be seen that the temperature within the lesion directly after the warm up time should be between 48 – 58°C, which is not unlikely since a coagulated area can be seen in Figure 23. The lesions in Table 8 are not exactly the same which is probably due to that different parts of

the bovine cardiac muscle have slightly different optical and thermal properties and that it is difficult to evaluate exactly where the lesion ends.

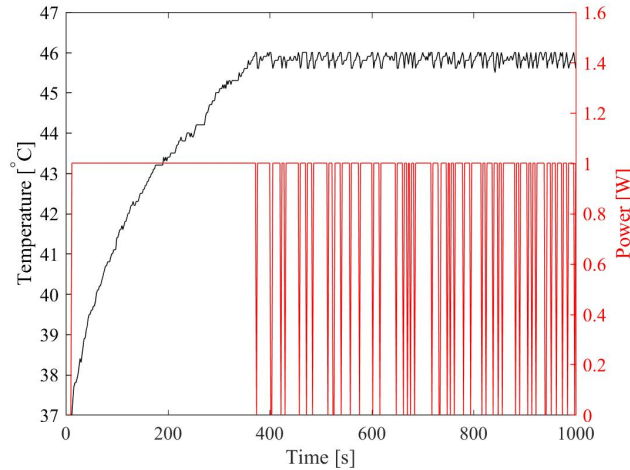


Figure 24: Left y-axis: A part of the temperature graph received from one of the validation experiments. It shows the temperature as function of time for a treatment using a bare end fiber with a source of 1 W and a distance between fiber and temperature probe of 5 mm. Right y-axis: Part of the power graph received from one of the experiments. The graph corresponds to the temperature graph in the figure.

The graph corresponding to the left y-axis (black) in Figure 24 shows the temperature in the tissue at a distance of 5 mm parallel to the fiber axis, slightly below the fiber tip, during the first half of a treatment. This when using a source of 1 W that is turned off when reaching the target temperature of 46°C and on when below this temperature. The corresponding power graph is shown in the right (red) part of Figure 24, where the ON-OFF behavior is clearly shown. This figure can be compared to Figure 21 and when comparing the left (black) graphs of them it can be seen that they both have a temperature that varies between 45.9-46.1°C but have different warm up times even though they start at the same temperature of 37°C. The warm up time for the simulation is 3 minutes and 54 seconds, and the average warm up time for the experiment is 5 minutes and 20 seconds. This difference can depend on a number of parameters, the temperature probe may have been placed in an area of either air or fat which would insulate the probe and give an incorrect read on the temperature, or the distance between fiber and temperature probe may not have been exactly 5 mm. Another possibility is that the scattering and absorption coefficients in the simulation do not correspond to that of the tissue used in the experiment. The last two are most likely since no irregularity was seen around the temperature probe when slicing the tissue after the experiment. Another reason for this conclusion is that the optical and thermal parameters are different for every bovine heart and may also differ for pieces of the same heart. This is also one of the reasons for why the warm up time is not the same for the last two experiments presented in Table 8.

The graphs corresponding to the right y-axes (red) of Figures 21 and 24 show the first half of a treatment of 30 minutes for the simulation and the first experiment respectively. The graphs look approximately the same, they both move from one to zero and back when the temperature measured at a distance of 5 mm is above or below 46°C respectively. An

indication of the fact that the temperature determines when to start or stop the laser is that the ON-OFF intervals in the power graphs are not equally spaced but correspond to high and low points in the temperature graph. This is also a verification of that the simulation of the ON-OFF behavior of the laser works for the heat distribution simulation model.

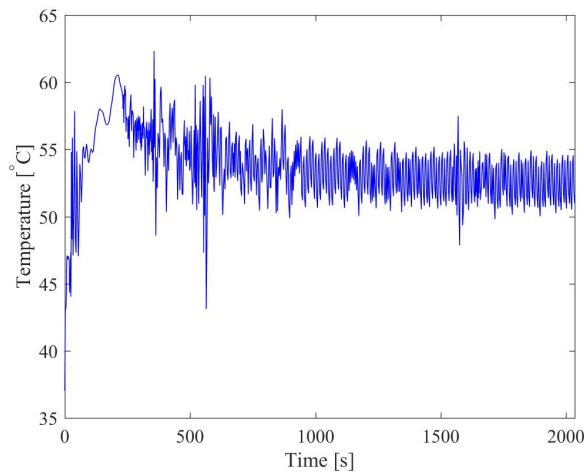


Figure 25: Temperature as a function of time for a point placed in the center of the core at the fiber tip.

The temperature in the core, shown in Figure 25, is on average 53°C with a peak of 62.5°C after approximately 360 s. Figure 26 shows the temperature as a function of time in the cladding of the fiber at the fiber tip. The graph shows the temperature for the entire simulation time and has a peak value of 68°C at 600 s. After this point in time the simulated temperature point has an average temperature of approximately 53°C . The temperature in the coating, shown in Figure 27 has an average value of 53°C and a peak temperature of 73°C at 600 s.

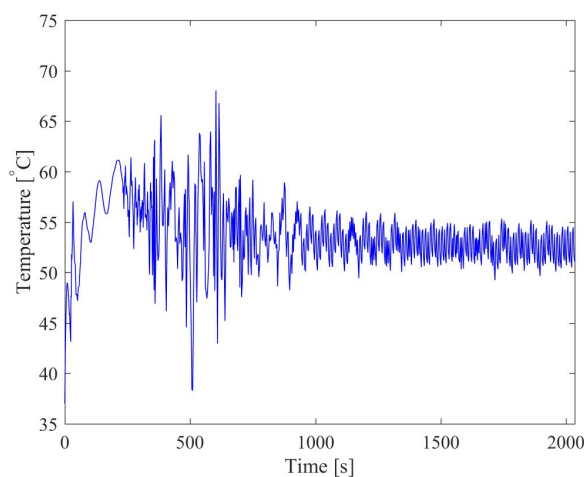


Figure 26: The temperature as a function of time in the cladding at the fiber tip.

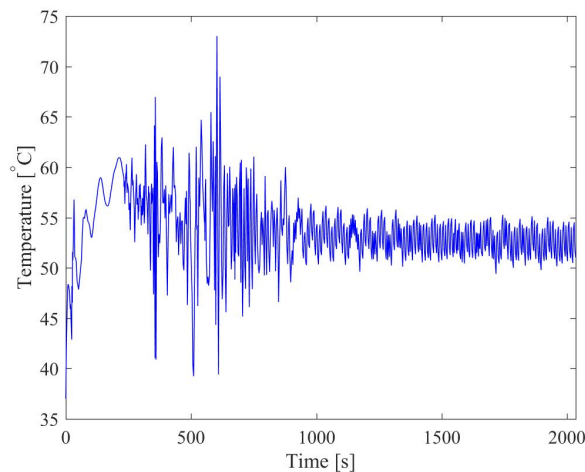


Figure 27: Temperature in the coating layer at the fiber tip as a function of time.

When comparing the temperature graphs shown in Figures 25-27 the same behavior through out the treatment time is seen. In the beginning the temperature varies a lot, less for the inner layers than for the outer, but still quite a bit. From a time of 600 s the temperature stabilizes around approximately 53°C with small variations. Temperature in the core varies approximately $5 - 10^{\circ}\text{C}$ in the beginning and is the smallest variation of the three layers. The largest temperature difference is for the coating layer, where the temperature varies approximately 40°C between 300 and 600 s. In reality the temperature varies in the different layers but it is unlikely that it varies as much as in the simulations. The reason for the large variation in the simulation could be due to that the diffusion approximation does not give a solution that is accurate closest to the fiber, it could also depend on the heat parameters used for the different layers.

4.3.2 Radial fiber

This section is divided into two parts, one for the treatment simulation and its corresponding experiments for fiber A and another for the burn simulations and experiments for both A and B. In the first section, the results from the imILT^{CLS} treatment simulation and experiment for fiber A is presented, and in the second section the results from the burn simulations and experiments are presented.

imILT^{CLS} model

In this section the results from the simulation of an imILT^{CLS} treatment is presented for fiber A. The wavelength and power used for both simulation and experiments are 1064 nm and 8 W respectively. The simulated time for fiber A during this part is 21 minutes and 48 seconds, which corresponds to a treatment time of 20 minutes and a warm up time of 1 minute and 48 seconds.

Figures 28- 30 show the results from the heat distribution simulation of radial fiber A and can be compared to those of the corresponding validation experiments, i.e. Figures 31 and 32. The first image is a slice of the 3D model which shows the heat distribution in the tissue and fiber.

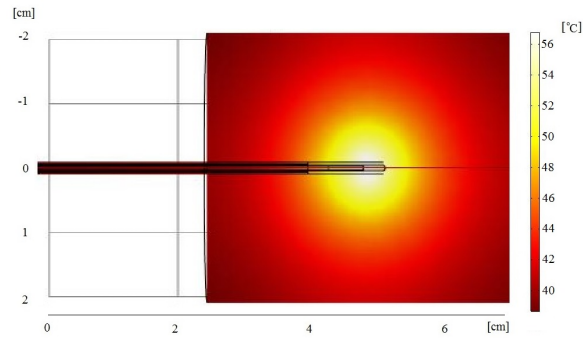


Figure 28: The heat distribution of radial fiber A at a wavelength of 1064 nm, a power of 8 W and a total simulated time of 21 minutes and 48 seconds. The colorbar represents the different temperatures in the image expressed in °C.

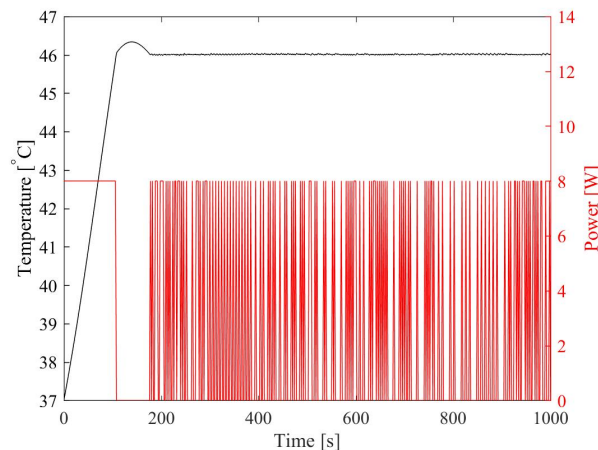


Figure 29: Left y-axis: The temperature as a function of time in the tissue at a distance of 10 mm from the fiber. This graph shows the temperature for approximately 17 minutes, when using a laser source of 1064 nm and 8 W. Right y-axis: Part of the power graph as function of time, received during a simulation of a treatment time of 20 minutes. The graph corresponds to the temperature graph in the figure.

The graph corresponding to the left y-axis (black) in Figure 29 shows the temperature in the tissue for a part of the total simulation time of 20 minutes, when simulating a source of 8 W that is turned off when reaching the target temperature of 46°C and on when below this temperature. Power as a function of time for a part of the total simulation time of 20 minutes is shown as the graph corresponding to the right y-axis (red) in Figure 29. The figure shows the ON-OFF behavior of the source due to the added step function in the heat source term. This image is compared to Figure 32, which corresponds to the temperature and power during one of the experiments.

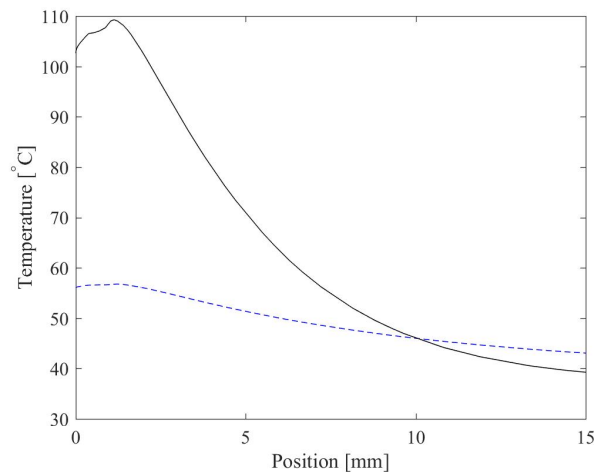


Figure 30: The temperature simulated at the fiber tip, from the center of the fiber and a few millimeters out in the tissue. The dashed graph corresponds to the temperature after 21 minutes and 48 seconds and the solid graph of a temperature after 1 minute and 48 seconds from the beginning of the simulation time, when using a source of 8 W and 1064 nm

Figure 30 shows the temperature at the center of the fiber core, at the plane of radiation and a few millimeters out in the tissue. The dashed graph in Figure 30 shows the temperature from the center of the fiber and out in the tissue for a treatment time of 20 minutes. From this graph it can be seen that the temperature in the simulation at the position of the lesion border in the experiments after 20 minutes corresponds to approximately 47°C in the simulation. This is the same as for the bare end fiber simulation and is a reasonable temperature since coagulation can occur at temperatures above 45°C. The damage caused during an *ex vivo* measurement is as said before caused to a great extent by the temperatures in the tissue directly after the warm up time ends. The temperature for the simulation for radial fiber A at this time is shown in the solid graph in Figure 30, where it can be seen that the temperature within the lesion volume in the simulation is between 105°C and 55°C. When comparing this to the image of the tissue for one of the experiments presented in Figure 31 it is not unreasonable that those are the temperatures also achieved during the experiments, but higher temperatures were expected in the simulation. The results are reasonable since carbonization in tissue is achieved at temperatures above 100°C causing the tissue to turn black and that coagulation occurs instantly for temperatures above 60°C. In Figure 31 it can then be seen that the tissue at the center of the lesion is turning black, which means that it is about to be carbonized, the discoloration directly outside of the part about to be carbonized in the same figure correspond to coagulated tissue.

Figure 31 shows an example of what the tissue may look like in the plane of the fiber after a treatment time of 30 minutes plus a warm up time of between 1 and 2 minutes and 30 seconds. An example of the placement of fiber and temperature probe during a treatment is also shown in Figure 31, which is represented by the two metal cylinders, where the left one represents the temperature probe and the right one, the fiber.

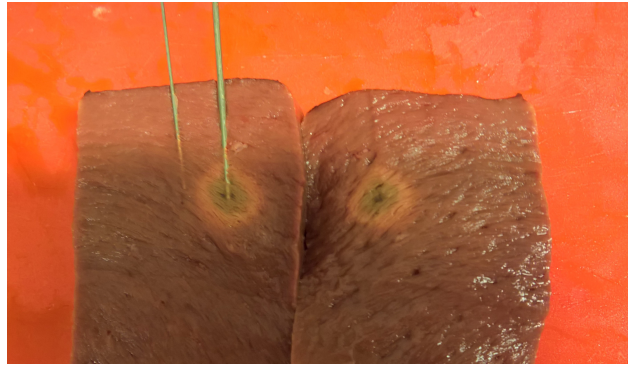


Figure 31: One result of a validation experiment using a radial fiber and a source of 8 W and 1064 nm for 30 minutes plus warm up time. The part of the tissue that is discolored is the area of the lesion caused by the treatment. The two metal cylinders in the image represents approximately where the fiber (right) and temperature probe (left) were placed and the distance between them is 10 mm.

Table 9 shows the results from the measurements made using the radial fiber. In the table, $T_{Initial}$ corresponds to the initial temperature of the tissue, t_{warmup} the warm up time, $t_{treatment}$ the treatment time and d_{lesion} the diameter of the lesion.

Table 9: Results from the treatment experiment for fiber A using a source of 8 W. *This time is shorter due to an error from the system causing the treatment to end.

$T_{Initial}$ [°C]	t_{warmup} [min:sec]	$t_{treatment}$ [min:sec]	d_{lesion} [mm]
36.0	1:30	30:00	16
37.9	1:22	30:00	15
37.5	2:08	23:04*	19
34.5	1:24	30:00	15

The lesion diameters from the validation experiments for fiber A presented in Table 9 corresponds to a treatment time of 30 minutes and can be compared to the temperature graph from the simulation presented in Figure 30. This comparison can be made since the result of the last 10 minutes of a 30 minute treatment time cannot be seen in *ex vivo* measurements since it is due to processes occurring in the tissue a time after the treatment and since the temperature in the tissue is approximately the same as for 20 minutes. After a treatment, the heat is distributed further out in the tissue causing cells further out than the immediate coagulation zone to be damaged to a point where it is easier for the body to kill them than to repair them. It is this response that is not seen in *ex vivo* measurements.

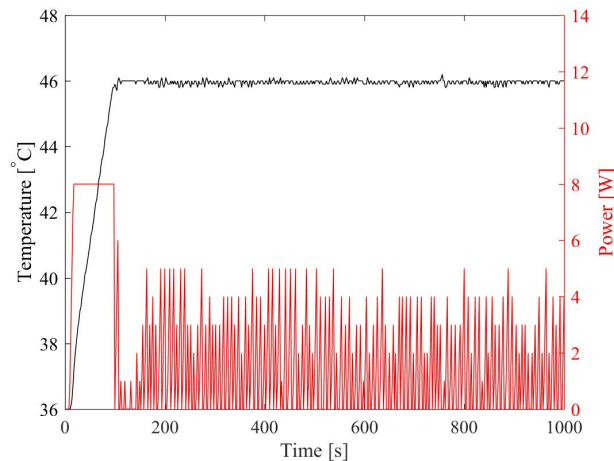


Figure 32: Left y-axis: The temperature graph received from one of the validation experiments corresponding to approximately half a treatment time of 30 minutes. It shows the temperature as function of time for a treatment using radial fiber A with a source of 8 W and a distance between fiber and temperature probe of 10 mm. Right y-axis: The power graph received from one of the experiments, which corresponds to the temperature graph on the left.

The left y-axis (black) of Figure 32 shows the temperature in the tissue at a parallel distance of 10 mm to the fiber axis and perpendicular to the core tip, during the first half of a treatment of 30 minutes plus warm up time. This when using a source of 8 W that is turned off when reaching the target temperature of 46°C and on when below this temperature. The corresponding power graph is presented by the right y-axis (red) of Figure 32, where the ON-OFF behavior is clearly shown. These graphs can be compared to those in Figure 32. The left graphs (black) in Figures 29 and 32 shows that the temperature in the tissue at a distance of 10 mm parallel to the fiber at the radiation point varies slightly around 46°C and have different warm up times but approximately the same initial temperature of 37°C. The warm up time for the simulation is 1 minute and 48 seconds, and the average warm up time for the experiment is 1 minute and 36 seconds. This difference depends on the same parameters as stated for the bare end fiber.

For the heat distribution simulation of radial fiber A it is also worth mentioning that the two power graphs to the right (red) in Figures 29 and 32 do not look the same. This is due to that when below 46°C in the simulation, the total power of 8 W is turned on immediately and in the experiment the power is instead delivered with a ramp up of 1 W/s until reaching 8 W. In the experiments the power does not reach 8 W again after the warm up time is over, since the temperature goes above 46°C before the power reaches 8 W. One result of this is that the average power of the simulation is approximately twice as much as that of the experiments during regulation. This is thus one possible source of error in the simulated heat distribution and could lead to a higher temperature in the tissue for the simulation than for the experiment and thus a larger treated volume.

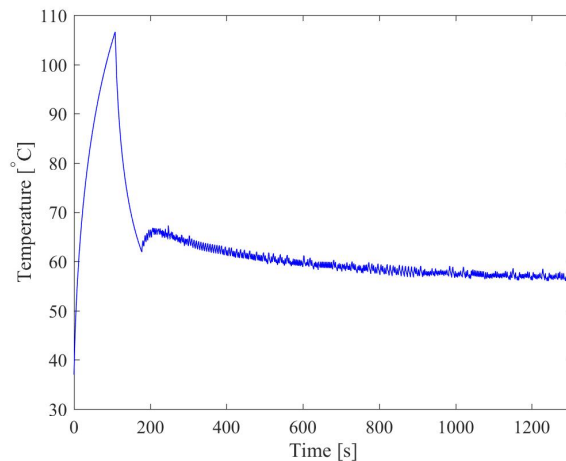


Figure 33: Temperature as a function of time for a point placed in the glass cap at the fiber tip for the simulation time of 21 minutes and 48 seconds using a source of 1064 nm and a power of 8 W.

The simulated temperature in the glass cap at the fiber tip, shown in Figure 33, is on average slowly decreasing but with a peak temperature of 106.6°C after 180 s. In Figure 34 the simulated temperature as a function of time in the glue inside the glass cap is presented. The graph shows the temperature for the entire simulation time and has a peak value of 59.8°C at 110 s. After 200 s the measurement point has an average temperature that decreases slowly with time.

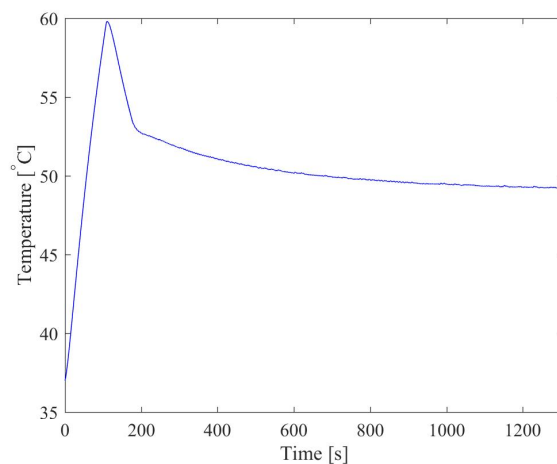


Figure 34: The temperature as a function of time for the point placed in the glue inside the glass cap for the simulation time of 21 minutes and 48 seconds using a source of 1064 nm and a power of 8 W.

When comparing the temperature graphs in Figures 33 and 34 the same behavior throughout the simulation time is seen for both simulation points. In the beginning both graphs present a large peak corresponding to the temperature during the warm up time, the temperature for the measurement point inside the glass of the cap has a peak temperature of approximately 107°C which is not unreasonable for the specific warm up time. The peak temperature of the simulation point in the glue inside the glass cap is approximately 60°C , which is not unreasonable, but since the heat parameters for this material are only an approximation the result should not be entirely trusted. After the peak the temperature

stabilizes and decreases slowly with time. Inside the glass cap wall the temperature after the peak is approximately 60°C , and at the glue the average temperature after the peak is approximately 50°C . The reason for the difference in average temperature as well as peak temperature for the two temperature points is mainly due to the placement of these points. For the glue inside the glass cap the temperature is lower since the distance to the irradiation plane is larger than for the point placed inside the glass of the cap. The temperature differences are partly due to the different thermal properties of the two materials as well as the thicknesses of the layers where the temperature points are placed.

Burn model

This section holds the results for the heat distribution simulations, or temperature simulations, for the two radial fibers when performing the simulations corresponding to the burn experiments in the lab. The simulation time for each fiber corresponds to the time it takes to burn each fiber in the lab. For fiber A, the burn time is 296 s and for fiber B, 144 s.

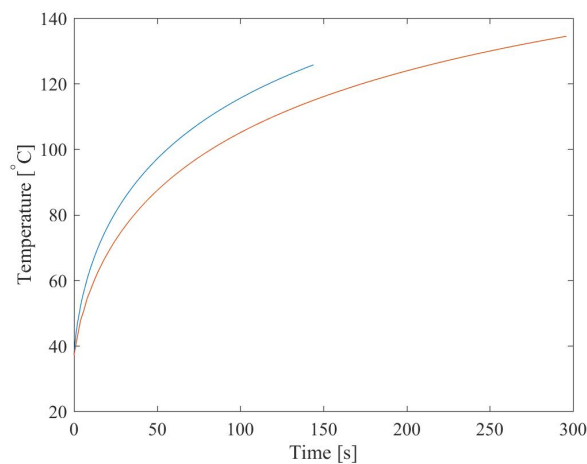


Figure 35: Temperature as function of time for the measurement point in the glass of the cap for fiber A and B. The red graph corresponds to fiber A and the blue to the results from fiber B.

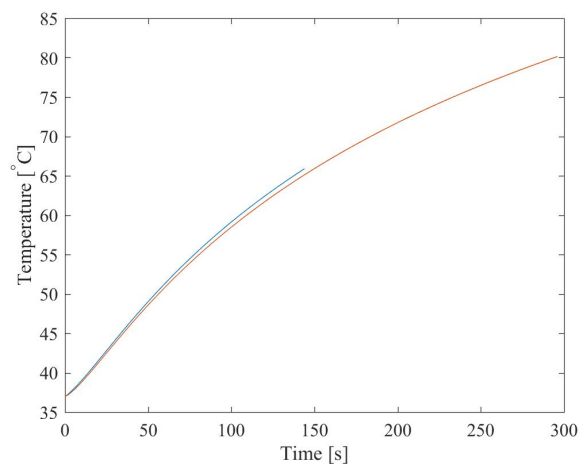


Figure 36: The two graphs show temperature against time for the measurement point in the glue placed inside the cap, for both fiber A and B. Fiber A corresponds to the red graph and fiber B to the blue one.

Figure 35 shows the temperature in side the glass of the cap perpendicular to the fiber at the place of radiation for fiber A and B. The red graph corresponds to the temperature of fiber A and the blue one to fiber B. The two graphs in Figure 36 correspond to temperature versus time in the glue placed inside the fiber cap for fiber A and B. Temperature in the glue for fiber A corresponds to the red graph in Figure 36. The blue graph in the figure corresponds to the temperature in the glue for fiber B.

One thing displayed in the graphs is that fiber A is simulated for a longer time than fiber B, which is done to simulate the temperatures for the time it takes to burn each fiber in the lab. These times are not entirely predictable since there are a number of factors that can affect them. One factor is the way of determining if the fiber has been burnt or not, the only way to do this is to observe the sample closely and turn off the laser when detecting smoke or a burnt scent. When performing the experiment for fiber A, no smoke was detected so the laser was turned off when a burnt scent was detected. For this experiment, small bubbles were detected in the PBS solution a while before the laser was turned off. This could have been an indication of that the fiber was burned and the smoke passed through small air channels inside the tissue and presented itself as bubbles instead of smoke. When performing the experiment for fiber B, smoke was detected before any other indication was noted. After examining the fiber when the experiment was completed it was only on the verge of being burned, meaning that the experiment could have been run for a longer time.

From the graphs in Figures 35 and 36 it can be seen that the temperature in the glass increases more rapidly for fiber B than for fiber A, but the temperature in the glue increases approximately at the same rate. This is an indication of that the thickness of the cap is an important parameter for the sustainability of the fiber and is most likely the parameter that determines maximum power and treatment time for fiber B. For fiber A this is not really the case since the glue only withstands a temperature of approximately 80°C which is the temperature for the glue at the last time step of the simulation. If the temperature from the simulation is correct then both glue and glass are important parameters for the sustainability of fiber A.

5 Discussion

From the results presented for the light and heat distributions, it can be seen that they are affected by the parameters μ_s , μ_a and g which in the literature vary depending on the article and measurement method used and is hard to find for a specific tissue type, in this case bovine cardiac muscle. These parameters can then cause some errors in the simulations of both the light distribution and the heat distribution. The errors cannot be discussed further for the light distribution since there are no validation experiments to compare with.

If μ'_s was to be increased the light would be distributed over a smaller area and the chance of absorption in this area would increase. Since it is the absorbed light that causes a temperature increase in the tissue, the increased probability of absorption also causes an increase in temperature. The same analysis can be made about the effects of the absorption coefficient, μ_a , if increased the tissue would have a faster warm up time but a smaller area of distribution.

It is not only the optical properties of the tissue that affects the thermal distribution but also the thermal properties such as, heat capacity, c , and thermal conductivity, k . The density, ρ , is also a factor affecting the thermal distribution in the tissue. The first parameter, c , is a property that defines the temperature change for a material in regards to the added heat. If the heat capacity is increased, the temperature will increase at a lower rate and a smaller area will be affected, and if decreased the opposite is expected. The second property affecting the heat distribution is the thermal conductivity, which is a property that defines how well a material can conduct heat. If this property is increased, the temperature in the material will increase at a lower rate but the affected area will be larger. The third parameter affecting the heat distribution is the density, if this parameter is increased the distribution area will decrease and the temperature in that area will also be decreased.

When moving forward with this model the parameters discussed in the paragraphs above are the ones that need to be determined more precisely. These parameters also change with temperature meaning that they also need to be changed continuously throughout the simulations to get a more precise approximation of reality.

The validations also need to be done in a better way. For the intensity distribution of the radial fiber, the validation could have been improved by evaluating the the profile at multiple positions around the cylinders and use the average of the results. Another possibility to improve the evaluation of the intensity profile of the radial fiber for the experiments is by doing multiple evaluations of the intensity width and use the average of that width. A third possibility of improving the validation of the intensity distribution of the radial fiber is to measure the angle of the fiber used in the validation and use that one for the simulation as well, this to see if the angle is what is incorrect or if the simulation model has other flaws. Improving the heat distribution validations could be made by using multiple temperature probes closer to the fiber during a treatment, thus measuring the temperature inside the treatment volume and compare that to the one received from the simulations. The validation of the burn simulations could have been improved by for example doing multiple experiments and use an average of the burn time in the simulations.

6 Conclusions and Outlook

The conclusions of this project is that it is possible to develop a simulation for an imILT^{CLS} treatment that to a great extent corresponds to reality. This project has only scratched the surface of the number of parameters that affect the lesion size achieved during a treatment and is thus only an approximation. For future work on this source model, the optical properties of the simulated tissue needs to be determined more precisely for the specific tissue under study since those are causing the largest errors in the current model. Changes in the optical properties due to coagulation and carbonization also needs to be added to get a better approximation of reality. The power protocol for the simulation of the radial fiber also needs to be reconsidered, since it does not correspond too well with the experimental data. Another thing that needs consideration is if diffusion is a good enough approximation for the light distribution, or if a more accurate approximation, such as Monte Carlo is needed.

7 Acknowledgments

First I would like to thank my two supervisors, Cristina Pantaleone and Johan Axelsson who have helped in any way they could to make this project possible. A second thanks goes to my temporary coworkers at CLS, for an enjoyable work environment. I would also like to thank Hampus M Jönsson, with whom I have made the validation experiments. Last I would like to thank my fiance who have supported me during this project.

8 References

- [1] C. Stureson. *Medical Laser-Induced Thermo-therapy - Models and Applications*. Ph.D. thesis, Lund University, (1998)
- [2] Clinical Laserthermia Systems AB. *imILT^{CLS}*. (2013)
URL: www.imilt.se (2016-08-31)
- [3] C. Pantaleone, S. Dyming, J. Axelsson. *Optical fiber solutions for laser ablation of tissue and immunostimulating interstitial laser thermo-therapy – Product development in the network of developers, industry and users* Photonics & Lasers in Medicine. Volume 5, Issue 1, pages 69–75. (2015)
- [4] D.F. Saldanha, V.L. Khatani, T.C. Carrillo, F.Y. Yap, J.T. Bui, M.G. Knuttinen, C.A. Owens and R.C. Gaba. *Current Tumor Ablation Technologies: Basic Science and Device Review* Seminars in interventional Radiology 27(3):247-54. (2010)
- [5] P. Saccomandi, E. Schena and S. Silvestri. *Design of fiber optic applicators for laser interstitial thermo-therapy: theoretical evaluation of thermal outcomes*. 35th Annual International Conference of the IEEE EMBS. 2013:3733-6. (2013)
- [6] L.V. Wang, H. Wu. *Biomedical Optics: principles and imaging*. John Wiley & Sons. pages 5-8. (2007)
- [7] V. Tuchin. *Tissue Optics: Light Scattering Methods and Instruments for Medical Diagnosis*. SPIE - The International Society for Optical Engineering. Vol. TT38. pages 3-8. (2000)
- [8] S.L. Jacques and B.W. Pogue. *Tutorial on diffuse light transport*. Journal of Biomedical Optics. Vol. 13(4). (2008)
- [9] A.J. Welch and M.J.C. van Gemert. *Optical-Thermal Response of Laser-Irradiated Tissue*. Springer. Second edition. pages 145-147 (2011)
- [10] T.H. Nguyen, S. Park, K.K. Hlaing and H.W. Kang. *Temperature feedback-controlled photothermal treatment with diffusing applicator: theoretical and experimental evaluations*. Optical Society of America. Vol. 7, No. 5. (2016)
- [11] A. Lakhssassi, E. Kengne and H. Semmaoui *Modified Pennes' equation modelling bio-heat transfer in living tissues: analytical and numerical analysis*. Natural Science. Vol.2, No.12, 1375-1385. (2010)
- [12] P. Saccomandi, E. Schena and S. Silvestri. *Design of fiber optic applicators for laser interstitial thermo-therapy: theoretical evaluation of thermal outcomes*. IEEE (2013)
- [13] D. Figueroa, C. Joshi, R. F. Wolf, J. Walla, J. Goddard, M. Martin, S. D. Kosanke, F. S. Broach, S. Pontius, D. Brown, X. Li, E. Howard, R. E. Nordquist, T. Hode, and W. R. Chen. *Interstitial laser immunotherapy for treatment of metastatic mammary tumors in rats* Biophotonics and Immune Responses VI. Proc. of SPIE Vol. 7900. (2011)

- [14] K. F. Chu and D. E. Dupuy. *Thermal ablation of tumours: biological mechanisms and advances in therapy*. NATURE REVIEWS | CANCER. Vol. 14. (2014)
- [15] K. H. Haraldsdóttir, K. Ivarsson, K. Jansner, U. Stenram and K.-G. Tranberg. *Changes in immunocompetent cells after interstitial laser thermotherapy of breast cancer*. Cancer Immunol Immunother 60:847–856. (2011)
- [16] B. M. Lippert, A. Teymoortash, B. J. Folz and J. A. Werner. *Coagulation and temperature distribution in Nd: YAG interstitial laser thermotherapy: an in vitro animal study*. Lasers Med Sci 18: 19–24. (2003)
- [17] C. Rossmann and D. Haemmerich. *Review of temperature dependence of thermal properties, dielectric properties, and perfusion of biological tissues at hyperthermic and ablation temperatures*. Crit Rev Biomed Eng. 42(6): 467–492. (2014)
- [18] COMSOL. *Ray Optics Module User's Guide*. Version 5.2. pages 83-85. (2015)
- [19] J. W. Fleming and D. L. Wood. *Refractive index dispersion and related properties in fluorine doped silica*. Applied Optics, Vol. 22, No. 19. (1983)
- [20] DuPont. *Kapton® polyimide film*. (2016)
URL: <http://www.dupont.com/products-and-services/membranes-films/polyimide-films/brands/kapton-polyimide-film.html/general/H-38479-4.pdf>
(2016-11-16)
- [21] Scientific Polymer Products, Inc. *Refractive Index of Polymers by Index*. (2013)
URL: <http://scientificpolymer.com/technical-library/refractive-index-of-polymers-by-index/> (2016-11-16)
- [22] THORLABS. *UV-Curing Optical Adhesives*. (2016)
URL: https://www.thorlabs.com/newgrouppage9.cfm?objectgroup_id=196
(2016-11-16)
- [23] Chemical Data Retrieval on the Web (CROW). *Polymer database: Poly(ether ether ketone)*. (2015)
URL: <http://polymerdatabase.com/polymers/polyetheretherketone.html>
(2016-11-21)
- [24] Goodfellow. *Polyethylene terephthalate (Polyester, PET, PETP)*. (2016)
URL: <http://www.goodfellow.com/E/Polyethylene-terephthalate.html> (2016-11-21)
- [25] F. P. Bolin, L. E. Preuss, R. C. Taylor, and R. J. Ference. *Refractive index of some mammalian tissues using a fiber optic cladding method*. Optical Society of America, Applied optics. Vol. 28, No. 12. (1988)
- [26] G. J. Muller, A. Rogga. *Laser-induced interstitial Thermotherapy*. Second edition, pages 28-40. Springer. (2011)
- [27] F.A. Duck. *Physical Properties of Tissues: A Comprehensive Reference book*. Academic Press: San Diego, CA, USA. page 28. (1990)

- [28] Chato, JC. *A method for the measurement of the thermal properties of biological materials*. In *Thermal Problems in Biotechnology*. JC Chato, ed., ASME symposium series, American Society of Mechanical Engineers, New York. (1968)
- [29] N. Akashi, J. Kushibiki, and N. Chubachi. *Acoustic properties of selected bovine tissues in the frequency range 20-200 MHz*. *Acoustical Society of America*, 98(6). (1995)
- [30] Accuratus. *Fused Silica, SiO₂ Glass Properties*. (2013)
URL: <https://accuratus.com/fused.html> (2016-11-16)
- [31] Crystran. *Silica Glass (SiO₂)*. (2012)
URL: <http://www.crystran.co.uk/optical-materials/silica-glass-sio2> (2016-11-16)
- [32] Professional Plastics *Thermal Properties of Plastic Materials*.
URL: <http://www.professionalplastics.com/professionalplastics/ThermalPropertiesofPlasticMaterials.pdf> (2016-11-16)
- [33] The Engineering Toolbox *Plastics - Thermal Conductivity Coefficients*.
URL: http://www.engineeringtoolbox.com/thermal-conductivity-plastics-d_1786.html (2016-11-16)
- [34] British Plastics Federation. *Plastipedia.co.uk: Nylons (Polyamide)*. (2016)
URL: <http://www.bpf.co.uk/plastipedia/polymers/polyamides.aspx> (2016-11-16)
- [35] Polytec. *Polytec UV 2108*. (2011)
URL: http://www.polytec.com/fileadmin/user_uploads/Polytec/Polytec_France/Produits/documents/Docs_techniques_Polytec_PT/Polytec_UV_2108_engl.pdf (2016-11-16)
- [36] AZO materials. *Supplier Data - Polyetheretherketone (PEEK) (Goodfellow)*. (2003)
URL: <http://www.azom.com/article.aspx?ArticleID=1882> (2016-11-28)
- [37] The plastics shop. *Product data sheet: Ketron 1000 PEEK*. (2011)
URL: http://www.theplasticshop.co.uk/plastic_technical_data_sheets/peek_1000_technical_data_sheet.pdf (2016-11-28)
- [38] J. Wen. *Chapter 9: Heat Capacities of Polymers*. ALZA Corporation.
- [39] Engineering Thermodynamics. *Specific Heat Capacities of Air*.
URL: https://www.ohio.edu/mechanical/thermo/property_tables/air/air_Cp_Cv.html (2016-11-28)
- [40] The engineering toolbox. *Air properties*.
URL: http://www.engineeringtoolbox.com/air-properties-d_156.html (2016-11-28)